S1. Technical description for RRKM/ME setup in the Multiwell 2023 program

There are some keywords related to the RRKM/ME computational setup specifically for the Multiwell 2023 program. The RRKM/ME simulations were mainly conducted by using the "CHEMACT" keyword, which enables the chemical activation of POZs with the excess energy from sesquiterpene ozonolysis. We also simulated the CI formation kinetics with a monoenergetic distribution of non-thermalized POZs by using the "DELTA" keyword (Text S5). All the RRKM/ME simulations were simplified by neglecting (1) the reverse reaction from CIs to POZs (keyword "NOREV"), (2) the tunneling in the POZ-to-CI conversion (keyword "NOTUN"), (3) the effects of intramolecular vibrational energy redistribution (IVR) which is expected to be slow (keyword "FAST"), and (4) the centrifugal correction (keyword "NOCENT"). The keyword "SUM" was used to obtain the sums of states from the external file generated by the Densum code in the package of the Multiwell 2023 program. For each POZ decomposition, 1000 simulations were conducted with the simulation timescale set by the "LOGT" keyword.

S2. Evidence that supports the assumption of steady-state SPC concentration

The main assumption in this study is the steady-state concentration of SPCs. Prior studies proposed that assuming steady-state SPC concentrations can fit the experimental data of OH-initiated oxidation kinetics of acetone across different temperatures within 237–353 K (Talukdar et al., 2003). Although the reaction may proceed from excited prereactive complexes (thereby skipping the SPCs) to directly reach the transition states, excited prereactive complexes may play a major role only at high temperatures (e.g., over 450 K for acetone) such that under atmospheric conditions the reactants tend to form SPCs (Yamada et al., 2003; Davis et al., 2005). The assumption of steady-state SPC concentrations also enables a computational simulation that

reproduces the experimentally observed temperature dependence of β-caryophyllene ozonolysis within 243–313 K (Ou and Chen, 2025). The agreement between the experimental measurements and the simulations suggests that the collision between reactants may primarily yield SPCs before the production of POZs .

S3. Derivation of the formation rate constant of CIs

This section describes the detailed derivation for the formation rate constant of CIs. For simplicity in the derivation, we firstly consider one CI from the ozonolysis of the sesquiterpene (SQT) molecule, wherein only one SPC and one POZ connect the reaction chain (Scheme II in the manuscript). For atmospheric chemistry models, the formation rate of CIs (R_f) is typically given by Eq. (S1).

$$R_f = k_{CI} \cdot C_{SQT} \cdot C_{O_3} \quad \text{(S1)}$$

Here k_{CI} is the formation rate constant of CIs generated from the reactions between sesquiterpene (SQT) and O_3, while C_{SQT} and C_{O3} represent the concentrations of SQT and O_3. If we change the perspective and start to think about the basic principle of elementary reactions, R_f is actually determined by the rate of POZ decomposition (Scheme II in the manuscript), and its expression is given by Eq. (S2).

$$R_f = k_3 \cdot C_{POZ} \quad \text{(S2)}$$

If we try to compare Eq. (S2) with Eq. (S1), we will find it necessary to express the concentration of POZ (C_{POZ}) as a function of C_{SQT} and C_{O3}. Based on Scheme II in the manuscript, the kinetics regarding the change of C_{POZ} along with ozonolysis time (t) can be analytically expressed as Eq. (S3).

$$\frac{dC_{POZ}}{dt} = k_2 \cdot C_{SPC} - (k_{-2} + k_3) \cdot C_{POZ} \quad \text{(S3)}$$

The quantity C_{SPC} represents the concentration of SPC and k_2 is the rate constant of POZ formation from the SPC. The generated POZ can either reversely produce SPC again or decompose into the CI, with the rate constants represented by k_{-2} and k_3, respectively. As supported by experimental studies (Talukdar et al., 2003; Davis et al., 2005; Ou and Chen, 2025), C_{SPC} can be approximated by its steady-state concentration (Eq. (S4)).

$$\frac{dC_{SPC}}{dt} = 0 \tag{S4}$$

Eq. (S4) means that, at any time during the SQT ozonolysis, the concentration of the SPC is assumed to be constant. The left-hand side of Eq. (S4), based on Scheme II in the manuscript, can be expressed as Eq. (S5).

$$\frac{dC_{SPC}}{dt} = k_1 \cdot p \cdot C_{SQT} \cdot C_{O_3} - (k_{-1} + k_2) \cdot C_{SPC} \tag{S5}$$

Here k_1 is the rate constant of effective collisions between the SQT and O_3, p is the branching ratio that the effective collisions can produce this SPC (as the SQT and O_3 indeed yield multiple SPCs), k_{-1} is the dissociation rate constant of the SPC, k_2 is the formation rate constant of the POZ from the SPC. Combining Eqs. (S4) and (S5), the steady-state concentration of SPC, denoted as $C_{SPC,ss}$, is given by Eq. (S6).

$$C_{SPC,ss} = k_1 \cdot p \cdot \left(\frac{1}{k_{-1}+k_2}\right) \cdot C_{SQT} \cdot C_{O_3} \tag{S6}$$

Eq. (S6) suggests that, within the modeling timescale, both the concentrations of SQT and O_3 are stable enough, so C_{SQT} and C_{O3} remain constant. It is noted that $C_{SPC,ss}$ is a function of temperature since k_1, k_{-1} and k_2 may change during the temperature variations. Substituting Eq. (S6) into Eq. (S3), we obtain Eq. (S7).

$$\frac{dC_{POZ}}{dt} = k_1 \cdot p \cdot \left(\frac{k_2}{k_{-1}+k_2}\right) \cdot C_{SQT} \cdot C_{O_3} - (k_{-2} + k_3) \cdot C_{POZ} \tag{S7}$$

For convenience, if we denote C_{POZ} as y, the first term on the right-hand side of Eq. (S7) as b, and $(k_{-2} + k_3)$ in Eq. (S7) as a, the Eq. (S7) then becomes a classical ordinary differential equation as shown in Eq. (S8).

$$\frac{dy}{dt} = b - ay \tag{S8}$$

After rearranging the Eq. (S8), we can conduct the indefinite integral as Eq. (S9), and then obtain the expression of y as a function of t with a constant c' for integration (Eq. (S10)).

$$\frac{1}{a} \cdot \int \frac{d(ay)}{b-ay} = \int dt \tag{S9}$$

$$y = \frac{b}{a} \cdot (1 - c'e^{-at}) \tag{S10}$$

Notably, in the experimental measurements of CI formation from ozonolysis, there is typically no pre-existing POZ (i.e., $y = 0$) when the ozonolysis starts (i.e., $t = 0$). In this case, we can obtain the value of c' by solving Eq. (S10), which provides $c' = 1$.

By transforming a and b back to their original symbols, the analytical expression of C_{POZ} is given by Eq. (S11).

$$C_{POZ} = k_1 \cdot p \cdot \left(\frac{1}{k_{-2}+k_3}\right) \cdot \left(\frac{k_2}{k_{-1}+k_2}\right) \cdot \left[1 - e^{-(k_{-2}+k_3)t}\right] \tag{S11}$$

Substituting Eq. (S11) into Eq. (S2), the analytical expression of R_f is given by Eq. (S12).

$$R_f = k_1 \cdot p \cdot \left(\frac{k_3}{k_{-2}+k_3}\right) \cdot \left(\frac{k_2}{k_{-1}+k_2}\right) \cdot \left[1 - e^{-(k_{-2}+k_3)t}\right] \cdot C_{SQT} \cdot C_{O_3} \tag{S12}$$

Now we obtain the formation rate of a single CI as a function of all the related rate constants of elemental reactions as well as the concentrations of SQT and O_3. Considering all the SPCs and their corresponding POZs generated from the ozonolysis and all the CIs generated from POZ decomposition, Eq. (S12) can be rewritten into a comprehensive expression given by Eq. (S13).

$$R_f = k_1 \cdot \sum_i \sum_j \left\{ p_i \cdot \left(\frac{k_{3,i,j}}{k_{-2,i}+k_{3,i,j}}\right) \cdot \left(\frac{k_{1,i} \cdot k_{2,i}}{k_{-1,i}+k_{2,i}}\right) \cdot \left[1 - e^{-(k_{-2,i}+k_{3,i,j})t}\right] \right\} \cdot C_{SQT} \cdot C_{O_3} \tag{S13}$$

The subscript i in Eq. (S13) indicates the i-th SPC and the i-th POZ, and the subscript j indicates the j-th CI from the i-th POZ decomposition. Both i and j are positive integers. The value of i ranges from 1 to the total number of CIs, while the value of j is either 1 or 2, since each POZ can decompose into two possible CIs. Comparing Eq. (S13) with Eq. (S1), we can directly obtain the expression of k_{CI}, which shows the rate constant of total CI formation (Eq. (S14)).

$$k_{CI} = k_1 \cdot \sum_i \sum_j \left\{ p_i \cdot \left(\frac{k_{3,i,j}}{k_{-2,i}+k_{3,i,j}} \right) \cdot \left(\frac{k_{1,i} \cdot k_{2,i}}{k_{-1,i}+k_{2,i}} \right) \cdot \left[1 - e^{-(k_{-2,i}+k_{3,i,j})t} \right] \right\} \quad \text{(S14)}$$

Eq. (S14) handles all the kinetic details at the "double-well" potential energy surface of the CI formation mechanism, and we indicate that Eq. (S14) can be simplified by two approximations. The first approximation is that k_{-2} may vanish, as it is negligibly small compared to $k_{3,i,j}$. This is because the energy barriers for the decomposition of POZs into SPCs are significantly higher than those for the CI formation (Donahue et al., 2011; Vereecken and Francisco, 2012; Taatjes et al., 2014). In this case, k_{CI} can be approximated by Eq. (S15).

$$\begin{aligned} k_{CI} &\approx k_1 \cdot \sum_i \sum_j \left[p_i \cdot \frac{k_{3,i,j}}{k_{3,i,j}} \cdot \left(\frac{k_{2,i}}{k_{-1,i}+k_{2,i}} \right) \cdot \left(1 - e^{-k_{3,i,j}t} \right) \right] \\ &= k_1 \cdot \sum_i \sum_j \left[p_i \cdot \left(\frac{k_{2,i}}{k_{-1,i}+k_{2,i}} \right) \cdot \left(1 - e^{-k_{3,i,j}t} \right) \right] \end{aligned} \quad \text{(S15)}$$

The second approximation is that the decomposition of each POZ produces only one major CI. Although there should be two CIs generated from the one POZ, one of the CIs has a faster formation rate, wherein the corresponding k_3 is several orders of magnitude higher than that of the other (Fig. S5). In this case, the summation based on j vanishes so that k_{CI} can be further approximated by Eq. (S16).

$$k_{CI} \approx k_1 \cdot \sum_i \left[p_i \cdot \left(\frac{k_{2,i}}{k_{-1,i}+k_{2,i}} \right) \cdot \left(1 - e^{-k_{3,i}t} \right) \right] \quad \text{(S16)}$$

The expression of k_{CI} in Eq. (S16) is very similar to the expression of k_{oz} (Eq. (1) in the manuscript). Their relationship can be clearly illustrated if we denote the branching ratio of the i-

th ozonolysis channel (i.e., the reaction pathway that generates the i-th CI through the i-th SPC and the i-th POZ) as r_i, which is given by Eq. (S17).

$$r_i = p_i \cdot \left(\frac{k_{2,i}}{k_{-1,i}+k_{2,i}}\right) \Big/ \sum_i \left[p_i \cdot \left(\frac{k_{2,i}}{k_{-1,i}+k_{2,i}}\right)\right] \quad \text{(S17)}$$

Eq. (S17) reveals that $\sum_i r_i = 1$. Substituting Eq. (S17) into Eq. (S16), the relationship between k_{CI} and k_{oz} can be derived as Eq. (S18).

$$\begin{aligned} k_{CI} &\approx k_1 \cdot \sum_i \left\{ r_i \cdot \sum_i \left[p_i \cdot \left(\frac{k_{2,i}}{k_{-1,i}+k_{2,i}}\right)\right] \cdot (1 - e^{-k_{3,i}t}) \right\} \\ &= k_1 \cdot \sum_i \left[p_i \cdot \left(\frac{k_{2,i}}{k_{-1,i}+k_{2,i}}\right)\right] \cdot \sum_i [r_i \cdot (1 - e^{-k_{3,i}t})] \\ &= k_{oz} \cdot \sum_i [r_i \cdot (1 - e^{-k_{3,i}t})] \end{aligned} \quad \text{(S18)}$$

Eq. (S18) provides a clear physical sense that, for the i-th CI, its formation rate constant can be estimated by the product of the ozonolysis rate constant and the time-dependent branching ratio projecting of this CI ($f_{CI,i}$), which is given by Eq. (S19).

$$f_{CI,i} = r_i \cdot (1 - e^{-k_{3,i}t}) \quad \text{(S19)}$$

Thus, the relationship between k_{CI} and k_{oz} can be written as Eq. (S20).

$$k_{CI} \approx k_{oz} \cdot \sum_i f_{CI,i} \quad \text{(S20)}$$

The time dependence of $f_{CI,i}$ shows the kinetic relaxation of k_{CI}. Eqs. (S19) and (S20) reveal that, when the ozonolysis begins (i.e., $t = 0$), the value of $f_{CI,i}$ is zero, which means that if the i-th POZ does not pre-exist, the initial formation rate constant of the i-th CI is zero, even though the ozonolysis rate constant of the SQT is the positive number k_{oz}. It is also noted that the value of $f_{CI,i}$ will unlimitedly approach r_i if the t is infinitely large (Eq. (S21)).

$$\begin{aligned} \lim_{t\to\infty} k_{CI}(t,T) &\approx \lim_{t\to\infty} \left[k_{oz}(T) \cdot \sum_i f_{CI,i}(t,T) \right] \\ &= k_{oz}(T) \cdot \lim_{t\to\infty} \sum_i f_{CI,i}(t,T) \end{aligned}$$

$$= k_{oz}(T) \cdot \lim_{t\to\infty} \sum_i [r_i \cdot (1 - e^{-k_{3,i}t})]$$

$$= k_{oz}(T) \cdot \sum_i r_i$$

$$= k_{oz}(T) \quad \text{(S21)}$$

Eq. (S21) indicates that k_{oz} represents the plateau value of k_{CI} if ozonolysis could proceed indefinitely. In the real atmosphere, k_{CI} is always in a state of deviation from k_{oz}, though it continuously tends toward this value.

S4. Formation rate constant of CIs with scale factors accounting for the pre-existing POZs

This section derives the analytical expression of k_{CI} if POZs pre-exist before the SQT ozonolysis starts. For convenience, we still start by considering only one CI produced from its corresponding POZ. The analytical expression of k_{CI} in Text S1 is derived based on the absence of pre-existing POZs, so that in Eq. (S10) the value of c' equals 1. If the initial concentration of this POZ is not zero, we may denote the value of its initial concentration as y_0 ($y_0 > 0$), and the value of c' can be obtained by solving Eq. (S10), which gives $c' = 1 - (y_0 \cdot a / b)$.

In the meantime, we also notice that, when t is infinitely large, the concentration of POZ unlimitedly approaches a constant, which is denoted as y_∞ in Eq. (S22).

$$y_\infty = \lim_{t\to\infty} \left[\frac{b}{a} \cdot (1 - c'e^{-at})\right] = \frac{b}{a} \quad \text{(S22)}$$

We find it more convenient to express c' as $c' = 1 - (y_0 / y_\infty)$, so Eq. (S10) transforms into a general expression of y, as shown in Eq. (S23).

$$y = y_\infty \cdot [1 - (1 - \frac{y_0}{y_\infty}) \cdot e^{-at}] \quad \text{(S23)}$$

In this case, if we define the scale factor (s) as the ratio of the initial POZ concentration to its ultimate value at an infinite t (i.e., $s = y_0 / y_\infty$ and $s > 0$), and transform y_∞, a and b back to their original symbols, the analytical expression of C_{POZ} with the scale factor will be given by Eq. (S24).

$$C_{POZ} = k_1 \cdot p \cdot \left(\frac{1}{k_{-2}+k_3}\right) \cdot \left(\frac{k_2}{k_{-1}+k_2}\right) \cdot \left[1 - (1-s) \cdot e^{-(k_{-2}+k_3)t}\right] \quad \text{(S24)}$$

Considering the formation of all the POZs and their CIs, along with the approximations discussed in Text S1, we further obtain the analytical expression of k_{CI} that accounts for the pre-existing POZs, as given by Eq. (S25).

$$k_{CI} \approx k_{oz} \cdot \sum_i \{r_i \cdot [1 - (1-s_i) \cdot e^{-k_{3,i}t}]\} \quad \text{(S25)}$$

Thus, the analytical expression of $f_{CI,i}$ becomes Eq. (S26).

$$f_{CI,i} = r_i \cdot [1 - (1-s_i) \cdot e^{-k_{3,i}t}] \quad \text{(S26)}$$

Eqs. (S25) and (S26) show that, when the ozonolysis begins (i.e., $t = 0$), the value of $f_{CI,i}$ is no longer zero but $r_i \cdot s_i$. Such a difference reveals that, if the i-th POZ pre-exists, the initial formation rate constant of the i-th CI is not yet zero. As s_i in Eq. (S26) is not considered as a time-independent quantity in this kinetic study, the value of k_{CI} with pre-existing POZs will unlimitedly approach k_{oz} if the t is infinitely large (Eq. (S27)).

$$\begin{aligned} \lim_{t\to\infty} k_{CI}(t,T) &\approx \lim_{t\to\infty}\left[k_{oz}(T) \cdot \textstyle\sum_i f_{CI,i}(t,T)\right] \\ &= k_{oz}(T) \cdot \lim_{t\to\infty} \textstyle\sum_i f_{CI,i}(t,T) \\ &= k_{oz}(T) \cdot \lim_{t\to\infty} \textstyle\sum_i \{r_i \cdot [1 - (1-s_i) \cdot e^{-k_{3,i}t}]\} \\ &= k_{oz}(T) \cdot \textstyle\sum_i r_i \\ &= k_{oz}(T) \end{aligned} \quad \text{(S27)}$$

Eqs. (S26) and (S27) indicate that, although pre-existing POZs may help reduce the gap between k_{CI} and k_{oz}, k_{CI} is still deviated from k_{oz}.

S5. RRKM/ME simulations starting from monoenergetic non-thermalized POZs

Decomposition kinetics of POZs was also explored by using the "DELTA" keyword, which set the initial distribution of POZs monoenergetically at the excess energy from sesquiterpene ozonolysis. These simulations took much longer computational time compared to those with chemical activation (i.e., the "CHEMACT" keyword). It turned out that a decrease in temperature for the monoenergetic simulations may significantly increase the computational time to even more than one week, and we found it almost impossible to finish the computation at below 300 K for all the sesquiterpene-derived POZs. We thus studied the temperature-dependent kinetics of POZ decomposition over 323−723 K (Tables S5 and S6), wherein the value of k_3 for each POZ was estimated by fitting the time-series data of their concentrations with the first-order decay model.

The value of k_3 for β-caryophyllene-derived POZs at atmospheric temperatures was evaluated according to the trend of k_3 values along with the simulation temperature. Our results showed that the k_3 values at different temperatures were well fitted by the modified Arrhenius equation (Figs. S11–S13). Our analysis mainly focused on the results at around 400 K, since the results at 400 K are close to the decomposition kinetics of POZs at atmospheric temperatures, as justified by the numerical instability in matrix inversions of RRKM/ME computation at lower temperatures (Chuong et al., 2004). In this case, the k_3 value of monoenergetic β-caryophyllene-derived POZs at atmospheric temperatures was estimated as ~10^{-3}–10^{-2} s^{-1} (Fig. S11). We also noted that further extrapolation of k_3 to 273 K and 298 K could be barely reliable; at these temperatures k_3 values are very close to those computed for the fully thermalized POZs (Table S7). Nevertheless, the k_3 values of β-caryophyllene-derived POZs are much smaller compared to those derived from other sesquiterpenes, which provides the β-caryophyllene-derived CI formation with the strongest kinetic relaxation.

Table S1. Comparison of computed POZ decomposition energy barriers between DLPNO-CCSD(T)/def2-TZVPP and DLPNO-CCSD(T)/cc-pVTZ (unit: kcal mol^{-1}).

Sesquiterpenes	DLPNO-CCSD(T)/def2-TZVPP		DLPNO-CCSD(T)/cc-pVTZ	
	CI1	CI2	CI1	CI2
α-cedrene	15.2	18.3	15.6	18.7
α-copaene	21.4	22.9	21.8	23.2
β-caryophyllene	27.6	25.8	28.1	26.3
α-farnesene	15.6	16.2	15.9	16.5
β-farnesene	16.4	19.2	16.9	19.5

Table S2. Fitted pre-exponential factors (*A*) of the Arrhenius equation based on the computational results of k_{-1} and k_2 for each SPC generated from the ozonolysis of α-cedrene and α-copaene.

SPC	α-cedrene		α-copaene	
	k_{-1}	k_2	k_{-1}	k_2
SPC1-1	1.6×10^{13}	4.2×10^{10}	1.6×10^{13}	9.3×10^{9}
SPC1-2	1.6×10^{13}	2.1×10^{10}	1.6×10^{13}	7.9×10^{9}
SPC2-1	1.6×10^{13}	2.1×10^{10}	1.6×10^{13}	5.7×10^{13}
SPC2-2	1.6×10^{13}	1.7×10^{10}	1.6×10^{13}	1.5×10^{13}

Table S3. Computed branching ratios of the ozonolysis channels of α-cedrene, α-copaene, and β-caryophyllene corresponding to different POZs across the studied temperatures.

T (K)	α-cedrene				α-copaene				β-caryophyllene*	
	1-1	1-2	2-1	2-2	1-1	1-2	2-1	2-2	3-1	3-2
243	0.00	0.00	0.94	0.06	0.00	0.00	0.66	0.34	0.52	0.48
248	0.00	0.00	0.94	0.06	0.00	0.00	0.65	0.35	0.52	0.48
253	0.00	0.00	0.93	0.07	0.00	0.00	0.65	0.35	0.51	0.49
258	0.00	0.00	0.93	0.07	0.00	0.00	0.64	0.36	0.51	0.49
263	0.00	0.00	0.93	0.07	0.00	0.00	0.63	0.37	0.50	0.50
268	0.00	0.00	0.93	0.07	0.00	0.00	0.63	0.37	0.49	0.51
273	0.00	0.00	0.92	0.08	0.00	0.00	0.62	0.38	0.49	0.51
278	0.00	0.00	0.92	0.08	0.00	0.00	0.62	0.38	0.48	0.52
283	0.00	0.00	0.92	0.08	0.00	0.00	0.61	0.39	0.48	0.52
288	0.00	0.00	0.91	0.09	0.00	0.00	0.60	0.40	0.47	0.53
293	0.00	0.00	0.91	0.09	0.00	0.00	0.60	0.40	0.47	0.53
298	0.00	0.00	0.91	0.09	0.00	0.00	0.59	0.41	0.46	0.54
303	0.00	0.00	0.90	0.10	0.00	0.00	0.59	0.41	0.46	0.54
308	0.00	0.00	0.90	0.10	0.00	0.00	0.59	0.41	0.46	0.54
313	0.00	0.00	0.90	0.10	0.00	0.00	0.58	0.42	0.45	0.55
318	0.00	0.00	0.90	0.10	0.00	0.00	0.58	0.42	0.45	0.55
323	0.00	0.00	0.89	0.11	0.00	0.00	0.57	0.43	0.44	0.56

*Estimated based on the computational results from Ou and Chen (2025).

Table S4. Relaxation timescale of CI formation from the thermalized POZs derived from α-copaene and β-caryophyllene.

T (K)	α-copaene (unit: hours)		β-caryophyllene (unit: days)	
	CI1	CI2	CI1	CI2
243	1576.1	9791.6	2.8×10^7	2.1×10^6
248	628.5	3635.0	9.0×10^6	6.8×10^5
253	259.7	1402.5	2.9×10^6	2.4×10^5
258	111.0	561.1	9.7×10^5	8.3×10^4
263	49.0	232.3	3.5×10^5	3.2×10^4
268	22.3	99.4	1.3×10^5	1.3×10^4
273	10.4	43.8	4.9×10^4	5000.0
278	5.0	19.9	1.9×10^4	2083.3
283	2.5	9.3	7638.9	902.8
288	1.2	4.4	3263.9	388.9
293	0.6	2.2	1388.9	180.6
298	0.3	1.1	631.9	83.3
303	0.2	0.6	284.7	39.6
308	0.1	0.3	131.9	19.4
313	0.06	0.2	64.6	9.7
318	0.03	0.1	31.9	4.9
323	0.02	0.05	16.0	2.6

Table S5. RRKM/ME-computed formation rate constant (unit: s^{-1}) of α-cedrene-derived, α-copaene-derived, and β-caryophyllene-derived CIs from non-thermalized POZ decomposition.*

T(K)	α-cedrene-derived CI1	α-cedrene-derived CI2	α-copaene-derived CI1	α-copaene-derived CI2	β-caryo-phyllene-derived CI1	β-caryo-phyllene-derived CI2
323	2.29×10^{2}	/	/	/	/	/
373	6.45×10^{3}	1.99×10^{2}	/	/	/	/
423	9.76×10^{4}	4.26×10^{3}	6.13×10^{1}	4.28×10^{1}	/	/
473	7.42×10^{5}	4.77×10^{4}	9.75×10^{2}	9.30×10^{2}	/	/
523	4.29×10^{6}	3.34×10^{5}	9.75×10^{3}	1.06×10^{4}	1.51×10^{1}	/
573	1.44×10^{7}	1.95×10^{6}	6.93×10^{4}	8.54×10^{4}	1.63×10^{2}	4.37×10^{2}
623	2.98×10^{7}	6.03×10^{6}	3.48×10^{5}	4.43×10^{5}	1.25×10^{3}	2.98×10^{3}
673	3.80×10^{7}	1.23×10^{7}	1.22×10^{6}	1.75×10^{6}	6.56×10^{3}	1.49×10^{4}
723	5.58×10^{7}	2.16×10^{7}	3.13×10^{6}	4.42×10^{6}	2.96×10^{4}	6.03×10^{4}

*Some values are not computed owing to the highly extensive simulation time.

Table S6. RRKM/ME-computed formation rate constant (unit: s^{-1}) of α-farnesene-derived and β-farnesene-derived CIs from non-thermalized POZ decomposition.*

T(K)	α-farnesene-derived CI1	α-farnesene-derived CI2	β-farnesene-derived CI1	β-farnesene-derived CI2
323	/	/	/	/
373	5.56×10^{3}	/	2.24×10^{3}	/
423	9.05×10^{4}	7.88×10^{3}	3.69×10^{4}	1.93×10^{3}
473	9.17×10^{5}	7.03×10^{4}	3.87×10^{5}	2.34×10^{4}
523	6.29×10^{6}	4.73×10^{5}	2.63×10^{6}	2.02×10^{5}
573	2.07×10^{7}	1.94×10^{6}	1.07×10^{7}	1.12×10^{6}
623	3.39×10^{7}	5.89×10^{6}	2.32×10^{7}	3.93×10^{6}
673	7.09×10^{7}	1.18×10^{7}	4.26×10^{7}	1.01×10^{7}
723	7.22×10^{7}	1.94×10^{7}	4.90×10^{7}	1.68×10^{7}

*Some values are not computed owing to the highly extensive simulation time.

Table S7. Comparisons of k_3 from mVTST computation and RRKM/ME-based extrapolation.

Sesquiterpene-derived CIs	k_3 from mVTST computation		k_3 from RRKM/ME-based extrapolation	
	273 K	298 K	273 K*	298 K*
α-cedrene-derived CI1	6.10×10^{0}	7.26×10^{1}	6.88×10^{-1}	1.49×10^{1}
α-cedrene-derived CI2	1.28×10^{-2}	2.42×10^{-1}	2.75×10^{-3}	9.83×10^{-2}
α-copaene-derived CI1	2.67×10^{-5}	8.19×10^{-4}	9.69×10^{-6}	4.14×10^{-4}
α-copaene-derived CI2	6.34×10^{-6}	2.54×10^{-4}	1.13×10^{-6}	7.79×10^{-5}
β-caryophyllene-derived CI1	2.38×10^{-10}	1.84×10^{-8}	2.15×10^{-10}	1.71×10^{-8}
β-caryophyllene-derived CI2	2.32×10^{-9}	1.40×10^{-7}	1.26×10^{-9}	9.18×10^{-8}

*Translational temperature of the colliders

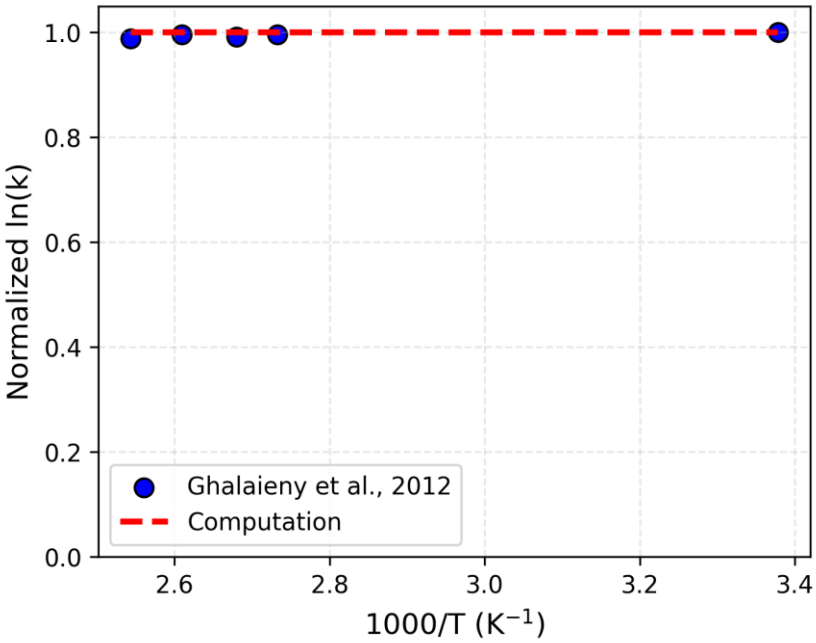


Figure S1. The experimental and computed ozonolysis rate constant of α-cedrene at different temperatures. The experimental data is reproduced with permission (Ghalaieny et al., 2012). Copyright 2012 Royal Society of Chemistry.

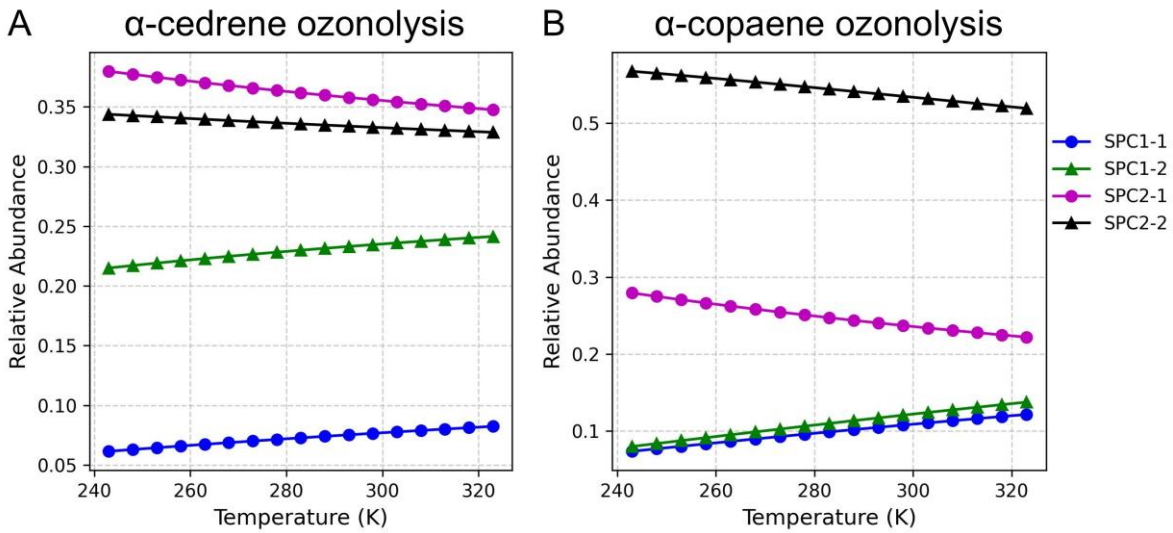
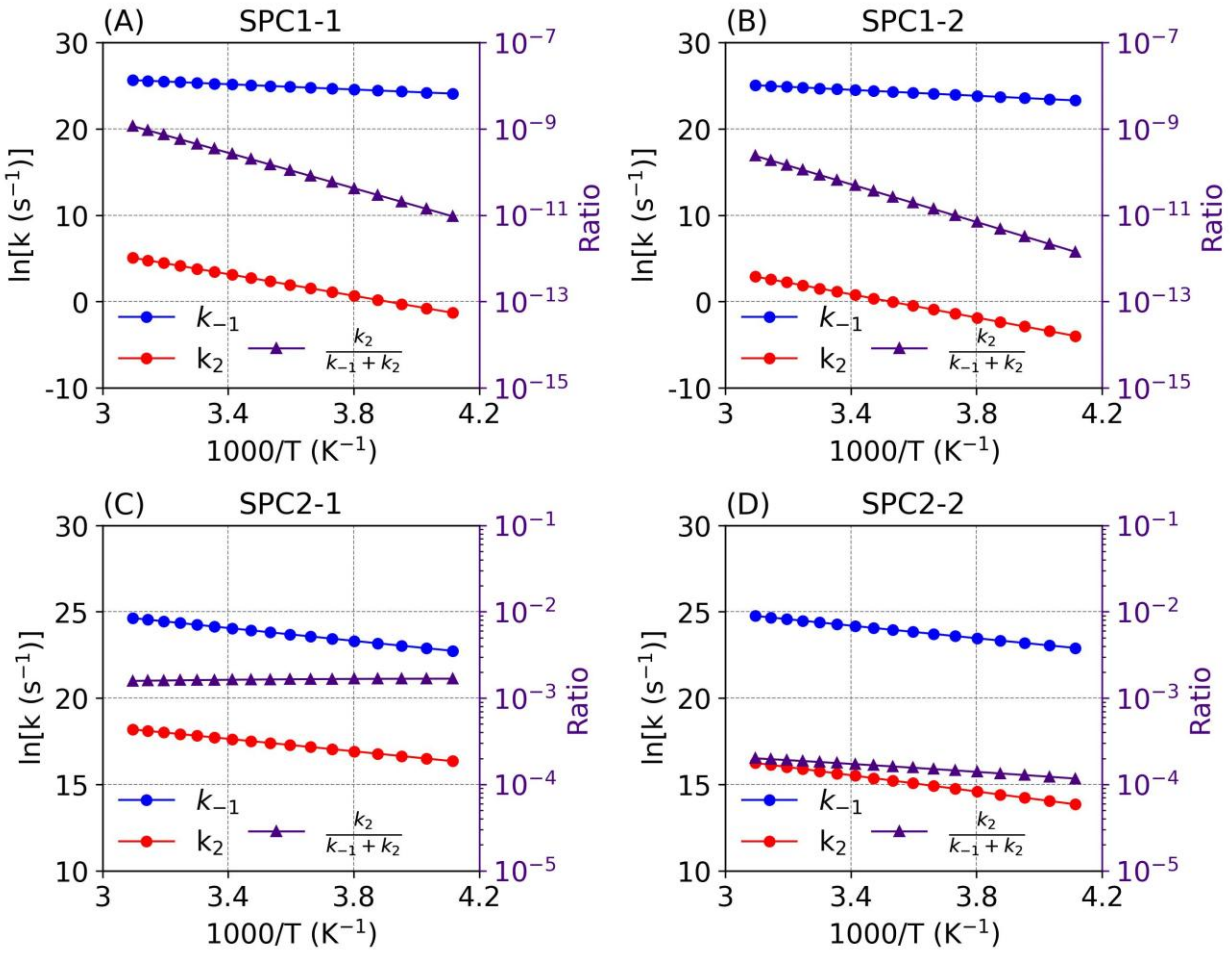


Figure S2. The relative abundance of SPCs in the ozonolysis of (A) α-cedrene and (B) α-copaene across the studied temperatures.



232

233 **Figure S3.** Temperature dependence of $ln(k_{-1})$, $ln(k_2)$ and $k_2 / (k_{-1} + k_2)$ of α-cedrene ozonolysis.

234

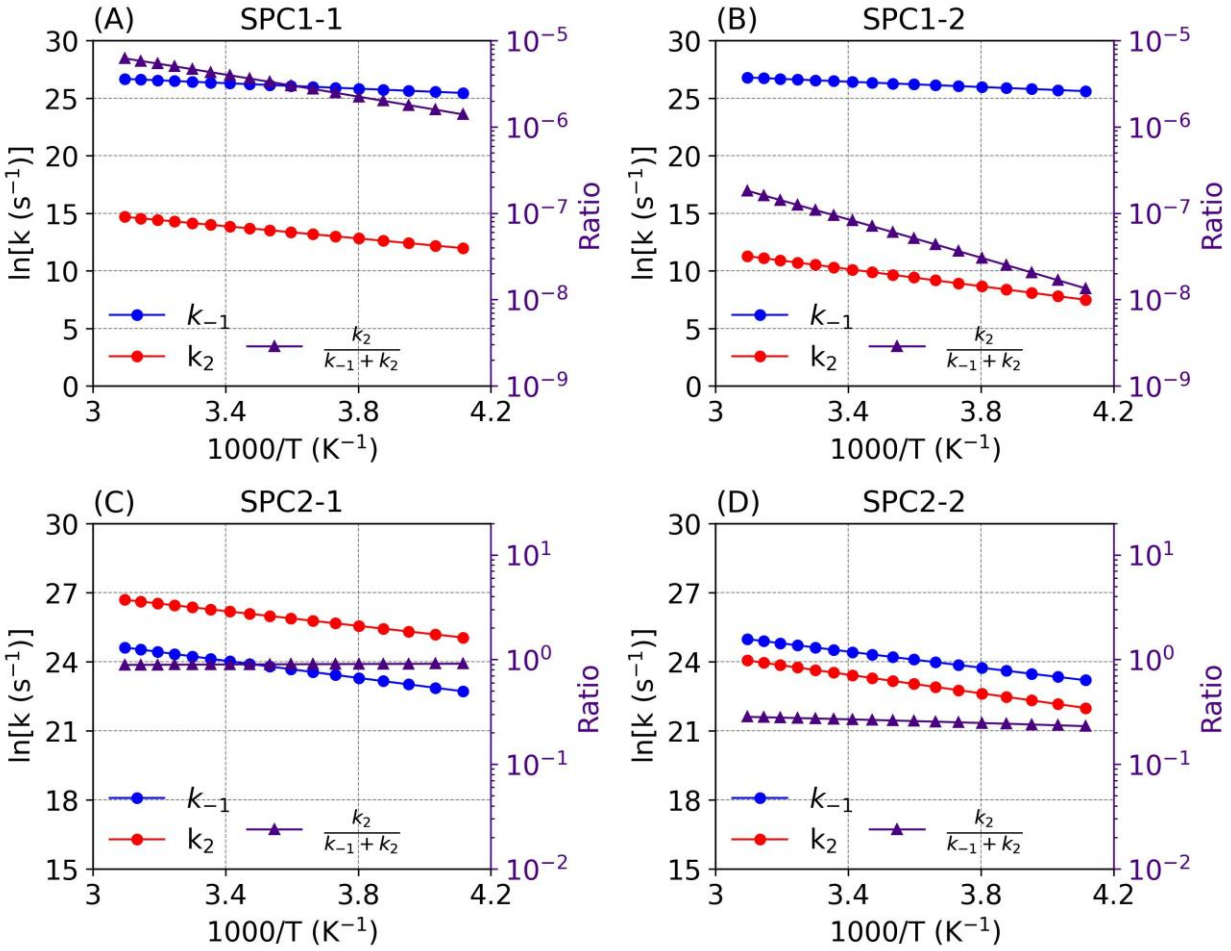


Figure S4. Temperature dependence of $ln(k_{-1})$, $ln(k_2)$ and $k_2 / (k_{-1} + k_2)$ of α-copaene ozonolysis.

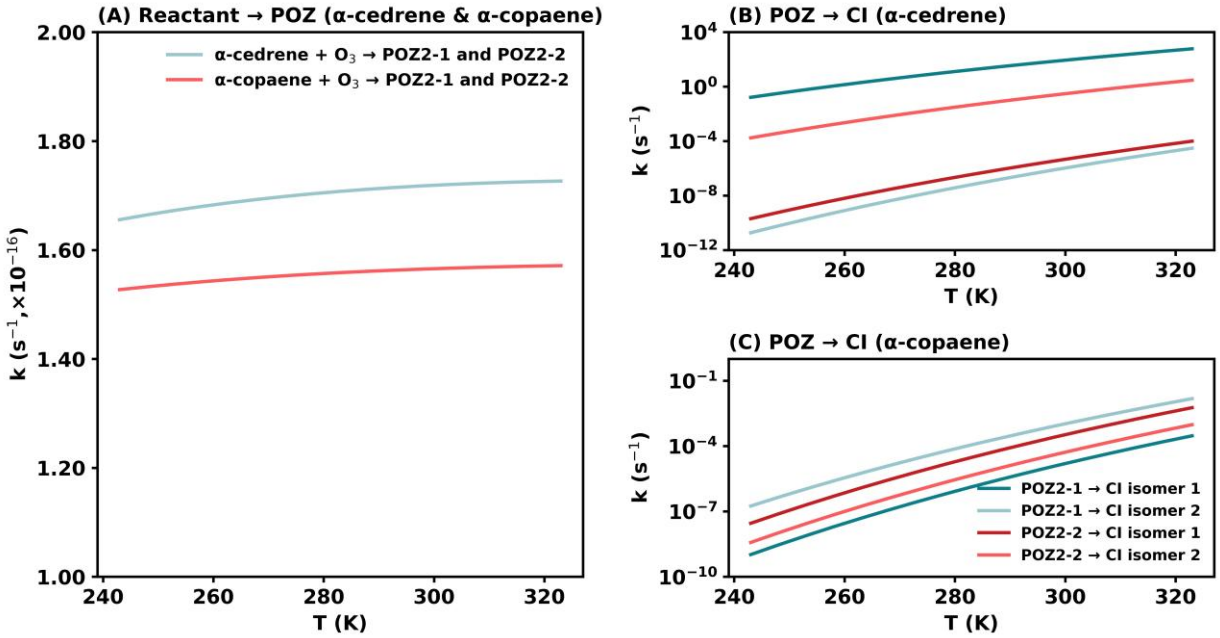
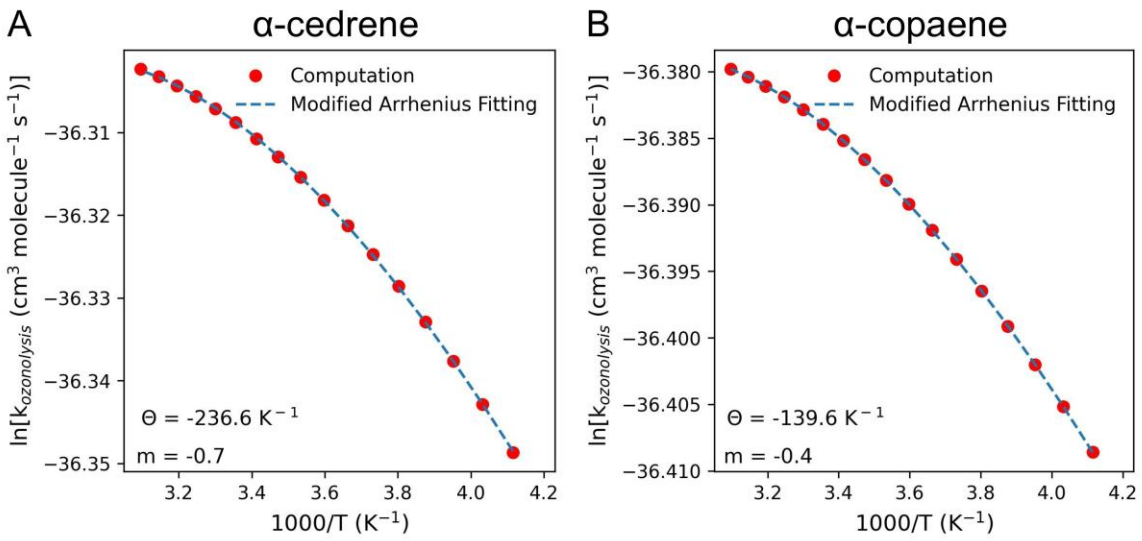


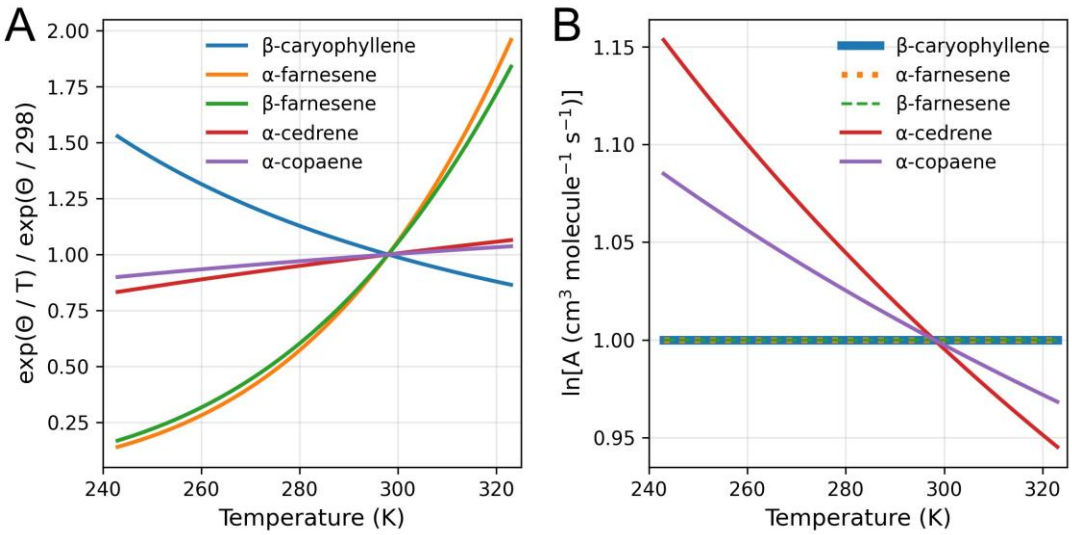
Figure S5. Temperature dependence of (A) the ozonolysis rate constants (k_{oz}) of α-cedrene and α-copaene and the decomposition rate constants (k_3) of thermalized POZs that produce (B) α-cedrene-derived CIs and (C) α-copaene-derived CIs.



243

244 **Figure S6.** Fitting of the computed temperature-dependent ozonolysis rate constants with the
245 modified Arrhenius equation.

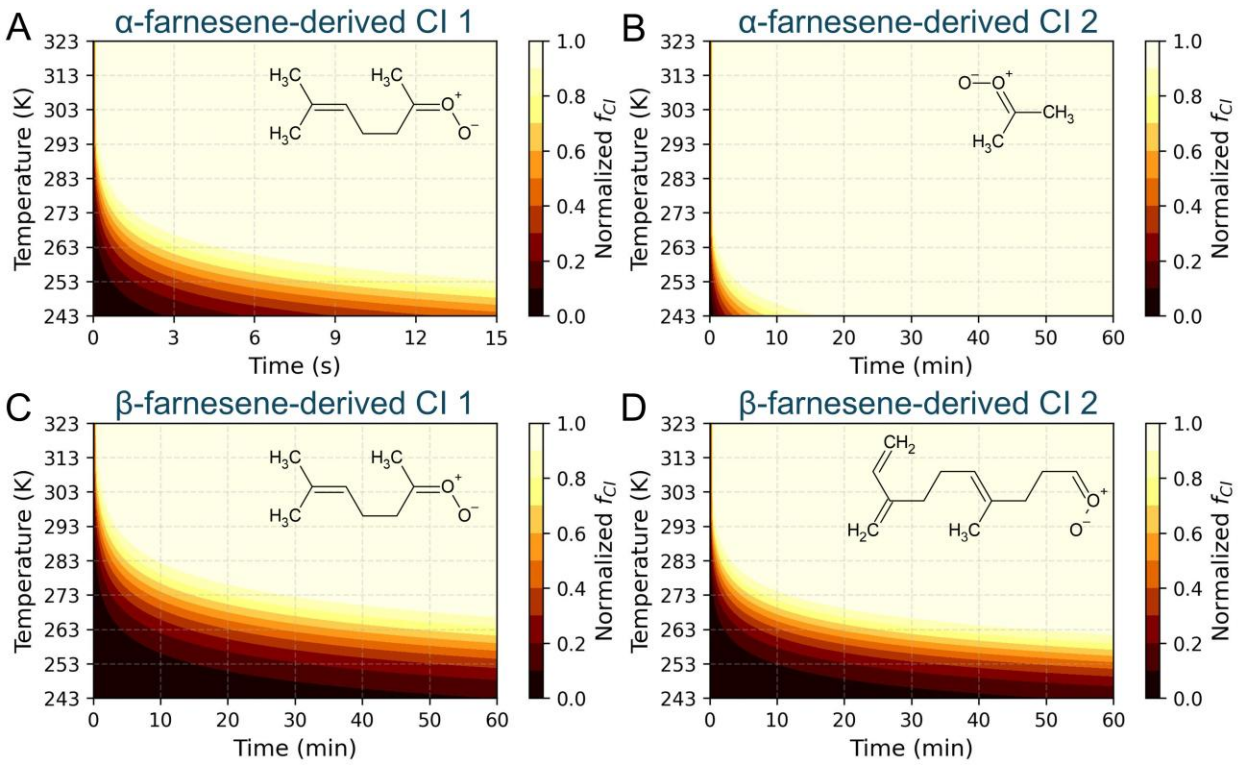
246



247

248 **Figure S7.** Comparison of Arrhenius equation components among β-caryophyllene (Gao et al.,
249 2022), α-farnesene (Kim et al., 2011), β-farnesene (Kim et al., 2011), α-cedrene, and α-copaene:
250 (A) relative exponential factor, and (B) pre-exponential factor (natural logarithm).

251



252

253 **Figure S8.** Kinetic relaxation of formation rate constant of (A) α-farnesene-derived CI1; (B) α-
254 farnesene-derived CI2; (C) β-farnesene-derived CI1; (D) β-farnesene-derived CI2.

255

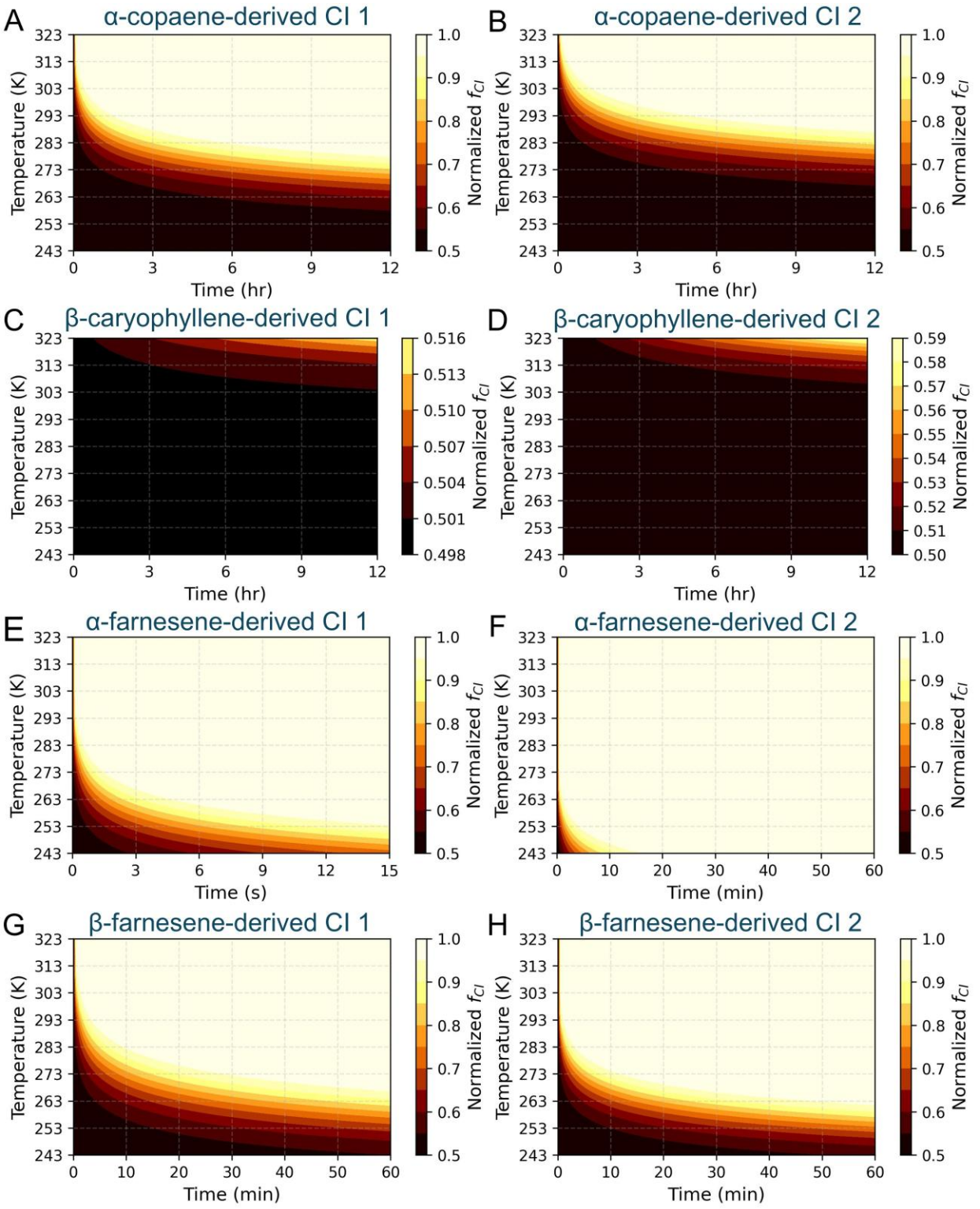
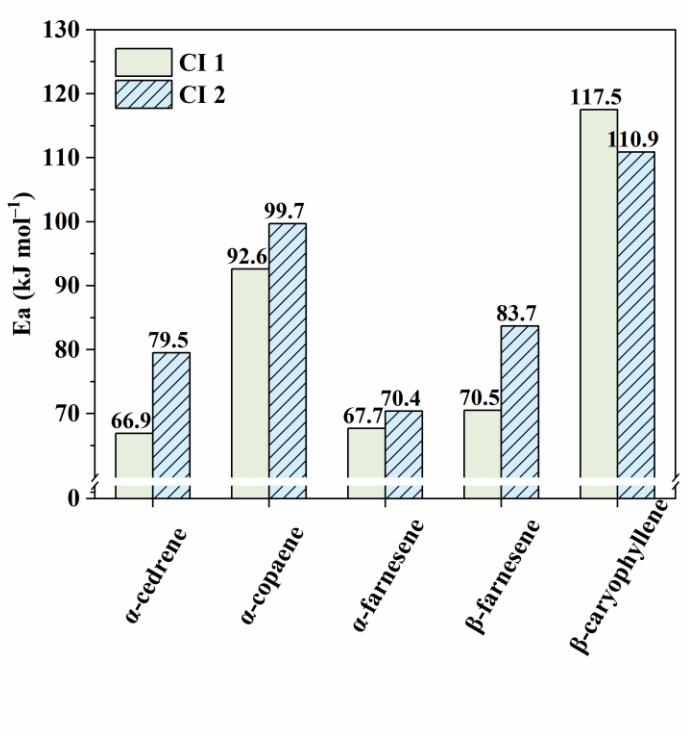


Figure S9. Kinetic relaxation of the modified k_{CI} with a scale factor of 0.5 for all the studied sesquiterpenes.



260

261 **Figure S10.** Activation energy of POZ decomposition rate constants (k_3) corresponding to CI1 and
262 CI2 of all the studied sesquiterpenes.

263

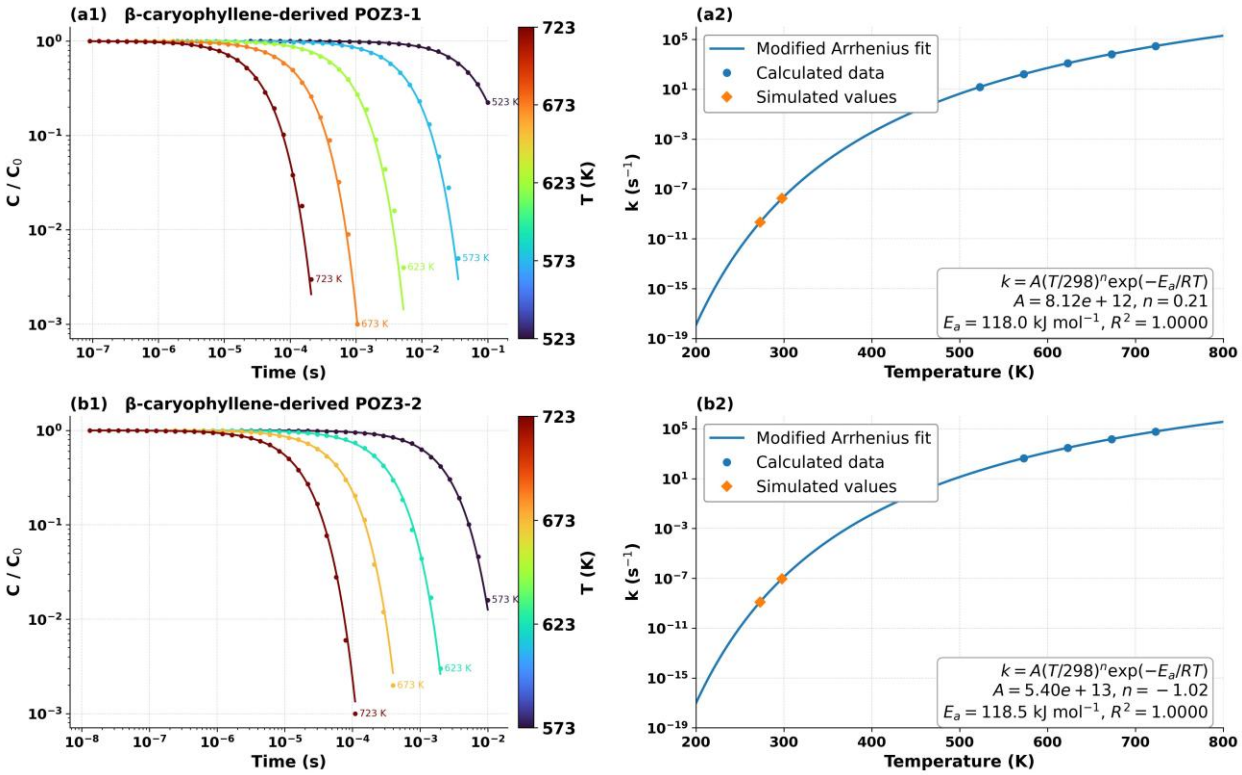


Figure S11. The normalized concentration (C / C_0) of β-caryophyllene-derived POZ3-1 (a1) and β-caryophyllene-derived POZ3-2 (b1) at different temperatures as directly output from the RRKM/ME computation. The structures of β-caryophyllene-derived POZ3-1 and POZ3-2 are obtained from our previous study (Ou and Chen, 2025); their decomposition produce β-caryophyllene-derived CI1 and CI2, respectively. The fitting k_3 results (a2-d2) are visulized with same order as the panels on the left.

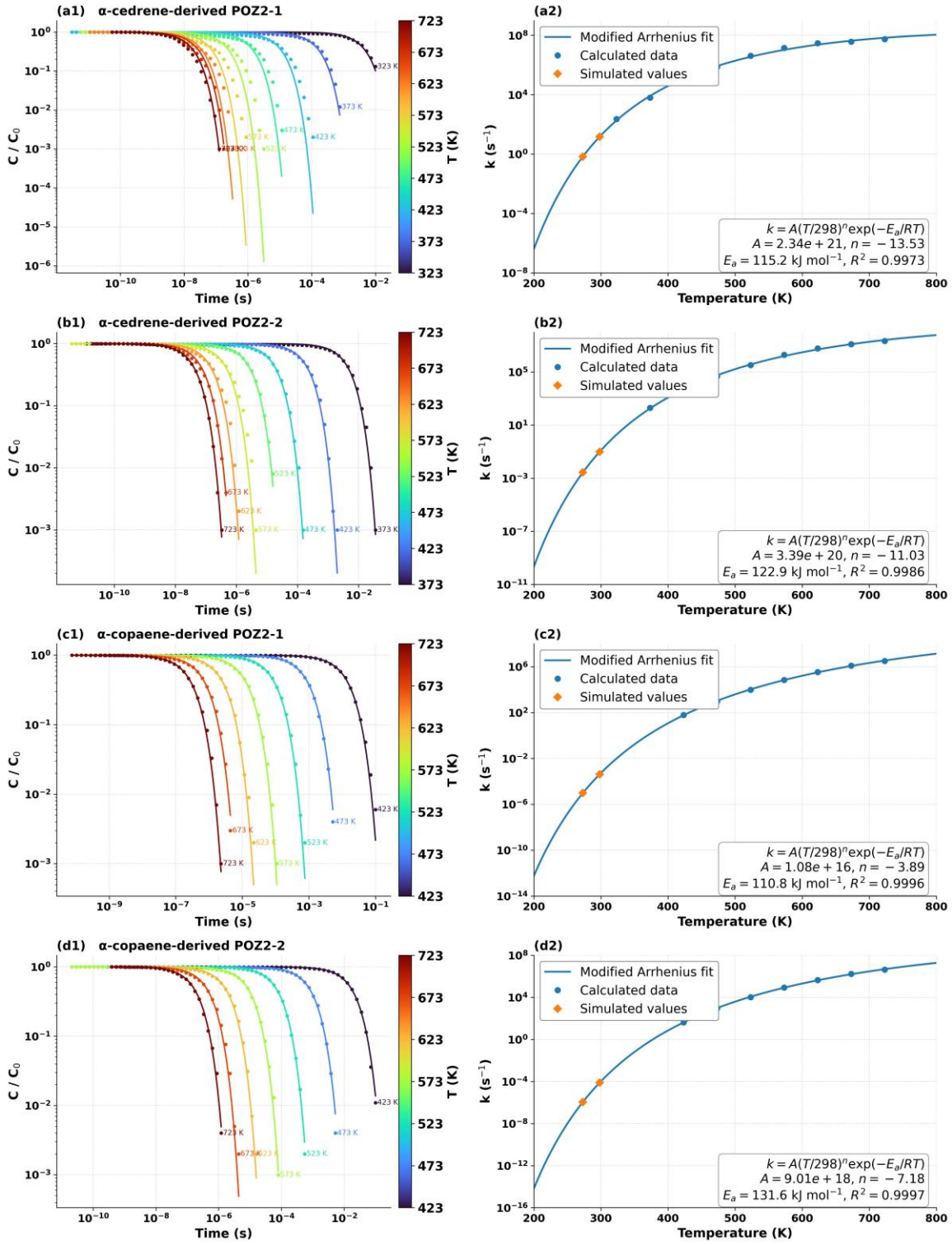


Figure S12. The normalized concentration (C / C_0) of α-cedrene-derived POZ2-1 (a1), α-cedrene-derived POZ2-2 (b1), α-copaene-derived POZ2-1 (c1) and α-copaene-derived POZ2-1 (d1) at different temperatures as directly output from the RRKM/ME computation. The fitting k_3 results (a2-d2) are visulized with same order as the panels on the left.

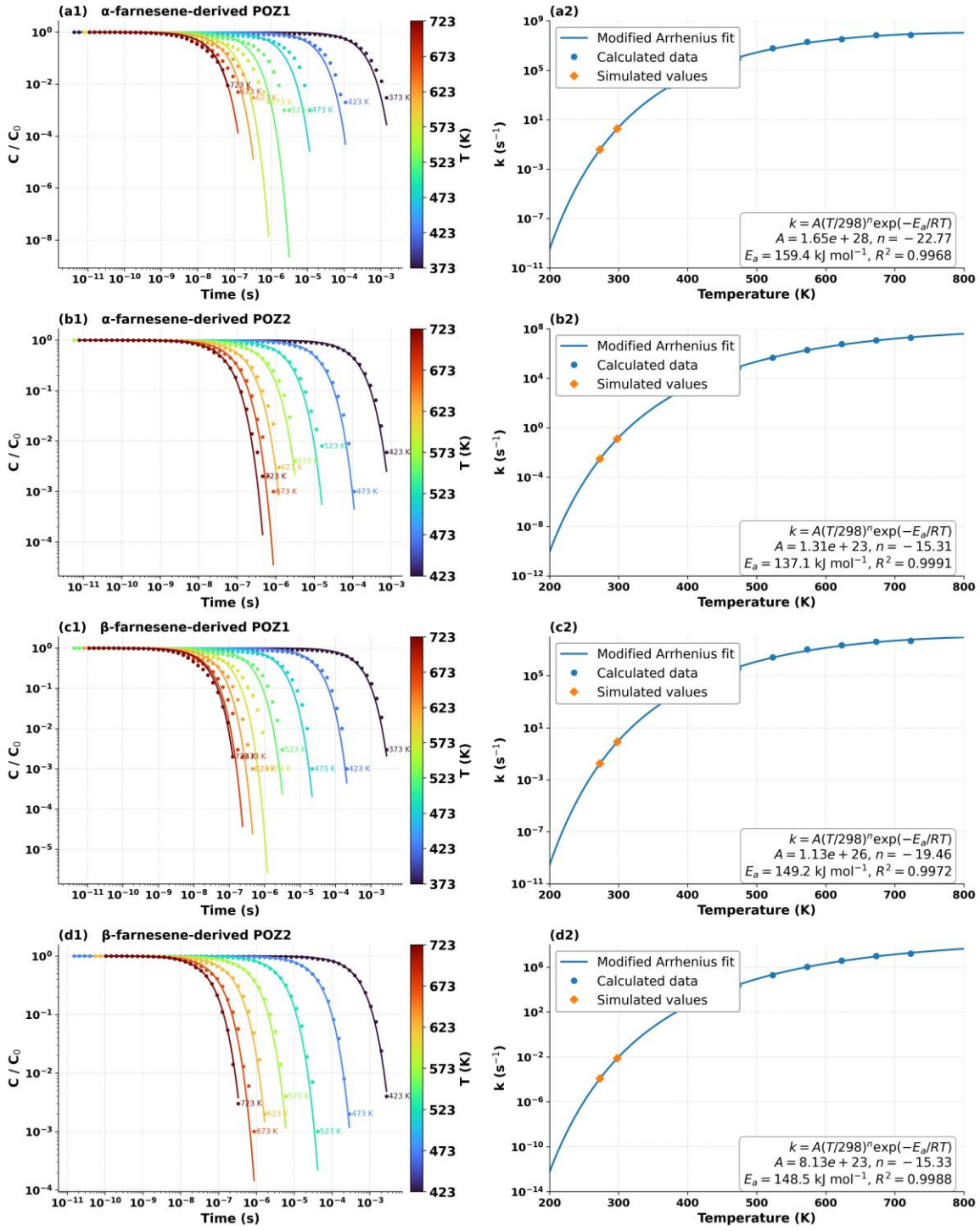


Figure S13. The normalized concentration (C / C_0) of α-farnesene-derived POZ1 (a1), α-farnesene-derived POZ2 (b1), β-farnesene-derived POZ1 (c1) and β-farnesene-derived POZ2 (d1) at different temperatures as directly output from the RRKM/ME computation. The fitting k_3 results (a2-d2) are visulized with same order as the panels on the left.

References

Chuong, B., Zhang, J., and Donahue, N. M.: Cycloalkene Ozonolysis: Collisionally Mediated Mechanistic Branching, J. Am. Chem. Soc., 126, 12363-12373, 10.1021/ja0485412, 2004.

Davis, M. E., Drake, W., Vimal, D., and Stevens, P. S.: Experimental and theoretical studies of the kinetics of the reactions of OH and OD with acetone and acetone-d6 at low pressure, J. Photochem. Photobiol. A Chem., 176, 162-171, https://doi.org/10.1016/j.jphotochem.2005.08.030, 2005.

Donahue, N. M., Drozd, G. T., Epstein, S. A., Presto, A. A., and Kroll, J. H.: Adventures in ozoneland: down the rabbit-hole, Phys. Chem. Chem. Phys., 13, 10848-10857, 10.1039/C0CP02564J, 2011.

Gao, L., Song, J., Mohr, C., Huang, W., Vallon, M., Jiang, F., Leisner, T., and Saathoff, H.: Kinetics, SOA yields, and chemical composition of secondary organic aerosol from β-caryophyllene ozonolysis with and without nitrogen oxides between 213 and 313 K, Atmos. Chem. Phys., 22, 6001-6020, 10.5194/acp-22-6001-2022, 2022.

Ghalaieny, M., Bacak, A., McGillen, M., Martin, D., Knights, A. V., O'Doherty, S., Shallcross, D. E., and Percival, C. J.: Determination of gas-phase ozonolysis rate coefficients of a number of sesquiterpenes at elevated temperatures using the relative rate method, Phys. Chem. Chem. Phys., 14, 6596-6602, 10.1039/C2CP23988D, 2012.

Kim, D., Stevens, P. S., and Hites, R. A.: Rate Constants for the Gas-Phase Reactions of OH and O3 with β-Ocimene, β-Myrcene, and α- and β-Farnesene as a Function of Temperature, J. Phys. Chem. A, 115, 500-506, 10.1021/jp111173s, 2011.

Ou, H. and Chen, K.: Atmospheric Temperature Dependence of β-Caryophyllene Ozonolysis Kinetics Is Governed by Stabilized Prereactive Complexes, J. Phys. Chem. A, 129, 9982-9990, 10.1021/acs.jpca.5c05523, 2025.

Taatjes, C. A., Shallcross, D. E., and Percival, C. J.: Research frontiers in the chemistry of Criegee intermediates and tropospheric ozonolysis, Phys. Chem. Chem. Phys., 16, 1704-1718, 10.1039/C3CP52842A, 2014.

Talukdar, R. K., Gierczak, T., McCabe, D. C., and Ravishankara, A. R.: Reaction of Hydroxyl Radical with Acetone. 2. Products and Reaction Mechanism, J. Phys. Chem. A, 107, 5021-5032, 10.1021/jp0273023, 2003.

Vereecken, L. and Francisco, J. S.: Theoretical studies of atmospheric reaction mechanisms in the troposphere, Chem. Soc. Rev., 41, 6259-6293, 10.1039/C2CS35070J, 2012.

Yamada, T., Taylor, P. H., Goumri, A., and Marshall, P.: The reaction of OH with acetone and acetone-d6 from 298 to 832 K: Rate coefficients and mechanism, J. Chem. Phys., 119, 10600-10606, 10.1063/1.1619950, 2003.